ACS OMEGA

Open Access

http://pubs.acs.org/journal/acsodf

Article

PFOS Exposure Promotes Hepatotoxicity in Quails by Exacerbating Oxidative Stress and Inflammation-Induced Apoptosis through Activating TLR4/MyD88/NF-κb Signaling

Jiucheng Wang,[#] Zanyu Wang,[#] Yulin Tang, Yuan Zhao, Hao Fang, Yuntong Zhang, Xiaoyu Hou, Haoyang Tan, Shiming Yu, Haiyang Zhang, Honggang Fan, Tianyuan Yang,[*] and Shuai Zhang[*]

Cite This: *ACS Omega* 2024, 9, 25370−25380

Read Online

ACCESS | Metrics & More | Article Recommendations | Supporting Information

ABSTRACT: PFOS is a ubiquitous pollutant garnering considerable attention due to its deleterious effects on both human and animal health. Given the poultry industry's intimate link with human health, investigating PFOS's impact on quails is crucial. PFOS readily accumulates in the liver, causing hepatotoxicity, yet its molecular mechanisms remain elusive. In our study, we fed quail diets contaminated with varying PFOS concentrations (12.5, 25, and 50 mg/kg) and observed dose-dependent liver damage in quails. The results show that PFOS damages mitochondrial structure, increases ROS levels, and downregulates antioxidants to promote oxidative stress damage in hepatocytes. PFOS also upregulated pro-inflammatory molecules (TNF-α, IL-1β, and IL-6) while downregulating the anti-inflammatory factor IL-10, activating the TLR4//MyD88/NF-κB signaling pathway, thereby potentiating liver inflammation. Then, oxidative stress and inflammation by PFOS induce apoptosis in quail hepatocytes through the mitochondrial pathway, with severity closely related to hepatotoxicity. In conclusion, PFOS induces mitochondrial apoptosis by exacerbating oxidative stress and inflammation by activating the TLR4/MyD88/NF-κB signaling pathway, ultimately leading to hepatotoxicity in quails.

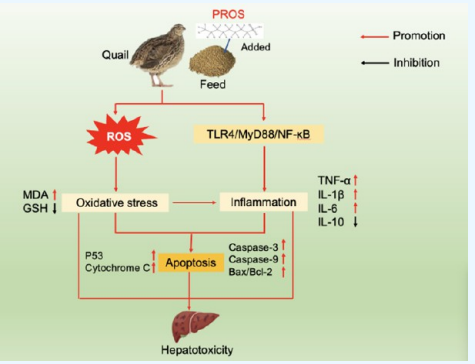

INTRODUCTION

Perfluorooctanesulfonate (PFOS), a major polyfluoroalkyl substance (PFAS), is known for its exceptional stability, particularly in terms of both thermal and chemical properties.[1] Since its invention by 3 M in 1949, PFOS has been widely used in various products, such as textiles, leather, and general cleaning products due to its oil and water-repellent properties and stability.[2,3] However, PFOS has recently been recognized as a persistent organic pollutant that is toxic, bioaccumulated, and resistant to biodegradation and photolysis.[4,5] As a result, the widespread use of PFOS and its ubiquitous presence in the environment pose a serious threat to ecosystem health and human well-being.

More and more studies have focused on the toxic effects of PROS on humans and animals. For example, PFOS persists in the environment and enters human systems through ingestion, exposure to PFOS products, and occupational exposure.[6] Simultaneously, PROS has the potential to interfere with the body's endocrine regulation, impede the reproductive functions of organisms, and weaken immunity.[7,8] In nature, PROS can be detected in the liver and blood of fish, birds, and mammals.[9,10] Particularly, birds that feed on fish and mammals show significant levels of PFOS in their tissues, such as ranging from 3 to 34 ng/mL in albatross serum in the central North Pacific.[11]

The liver, a vital organ for digestion and metabolism, accumulates PFOS more than any other organ.[12] As a key toxin filter, the liver is highly susceptible to PFOS-induced hepatotoxicity. Research has shown that PFOS exposure can cause hepatomegaly and liver toxicity in animals.[13] Simultaneously, PFOS can cause hepatocyte apoptosis and interfere with the activity of some cellular enzymes, ultimately leading to liver damage and dysfunction.[14] However, the mechanism of PFOS accumulation-induced hepatotoxicity is still not completely clear.

PFOS can induce hepatotoxicity in a variety of ways, including inflammation and oxidative stress.[15−17] As a key pro-inflammatory regulator, NF-κB can be activated by various inflammatory stimuli to increase the expression of inflammatory factors, such as IL-1β, IL-6, and TNF-α in the liver.[16,18,19] PFOS has been found to facilitate the activation of the NF-κB signaling pathway to induce inflammation in C6 glioma cell lines.[20] At the same time, PFOS can also directly damage

Received: April 19, 2024
Revised: May 17, 2024
Accepted: May 21, 2024
Published: May 31, 2024

hepatocyte mitochondria, disrupting the electron transport chain and releasing toxic reactive oxygen species (ROS), leading to hepatotoxicity.[21,22] The liver is particularly sensitive to ROS-induced oxidative stress. Additionally, PFOS causes oxidative damage in the liver by inducing ROS formation and depleting antioxidant defenses. Excessive ROS-induced oxidative stress triggers downstream apoptotic effects.[23] A valuable study found that PFOS causes cells to cause cellular dysregulation of oxidative homeostatic change, leading to abnormal apoptosis in the human embryo liver L-02 cells.[21] However, it remains unclear the mechanism of PFOS-induced hepatotoxicity in quail.

Therefore, we aim to investigate whether PFOS exposure promotes hepatotoxicity in quail by exacerbating oxidative stress and inflammation-induced apoptosis by activating TLR4/MyD88/NF-κB signaling. These results will provide insights into the signaling pathways behind PROF's hepatotoxicity in quail and could be promising strategies for further research.

MATERIALS AND METHODS

Experimental Animals. 30 adult female quails (Coturnix japonica, 110 ± 20 g) aged 35 days were provided by Wan Jia Poultry Farm (Harbin, China). After completing the general clinical examination and quarantine, the quails were then evenly divided into five metal cages and given free access to purified water and quail-specific pellet feed (contains corn, soybean meal, fish meal, bone meal, Vinoquail dovetail, Vinozyme, and Vinozyme complex probiotics). All quails were raised under standard laboratory conditions at the Laboratory Animal Center of Northeast Agricultural University (Harbin, China). The room was cleaned to maintain a good feeding environment at 8:00 each morning. Briefly, the temperature dimension of the feeding environment should be maintained at 26 ± 2 °C, humidity 55 ± 5%, and light should be maintained at 12 h of light/12 h of darkness. The Northeast Agricultural University's Animal Ethics Committee oversaw and approved all animal procedures (SRM-11, China).

Experimental Design. All quails were acclimated for 1 week before starting official trials and then placed into five groups at random (n = 6 per group): (1) the control group (Con): consuming food and liquids without restriction; (2) the control group with vehicle (Vcon): 150 mL of 2% Tween 80 (Solarbio, Beijing, China) solution was added to 7 kg of quail feed; (3) the low dose of PFOS group (LP); (4) the moderate dose of PFOS group (MP); and (5) the high dose of PFOS group (HP): 78.6, 175.2, and 350 mg of PFOS were dissolved in 150 mL of 2% Tween 80 solution, and then evenly mixed with 7 kg of standard feed and dried. The final concentrations of PFOS in the feed were 12.5 mg/kg (LP), 25 mg/kg (MP), and 50 mg/kg (HP).

Sample Collection. All quails were anesthetized with 1.5% isoflurane (Rayward Biotechnology, Shenzhen, China) after 42 days of feeding with the method mentioned above and then sacrificed. Afterward, blood samples were taken from the heart and placed at room temperature for 30 min. The centrifuge was then operated at 4 °C and a speed of 3000 r/min for 10 min. The serum was gathered and preserved at a temperature of −80 °C for future analysis of liver function indicators, lipid levels, and inflammatory markers in the serum. The abdominal skin was cut to expose the abdominal cavity. The liver was carefully removed and sectioned with a surgical scalpel. The appearance and dimensions of all the quail livers are shown in Supporting Information Figure 1. Part of the liver tissue blocks were fixed in a 4% paraformaldehyde fixating solution and stored at 4 °C for morphological observation and immunohistochemical test after the paraffin embedding section. The other part of the tissue was frozen at −80 °C for subsequent western blot assay and detection of oxidative stress and lipid metabolism-related kit. Some liver tissues were frozen in liquid nitrogen and transferred to −80 °C for real-time PCR. A separate portion of liver tissue was subjected to fixation using a 2.5% glutaraldehyde solution to conduct transmission electron microscopy analysis to examine the alterations in the ultrastructure of hepatocytes.

Assessment of Liver Function. Liver function was assessed by measuring the levels of aspartate aminotransferase (AST), alanine aminotransferase (AL), and gamma-glutamyl transferase (γ-GT). AST, ALT, and γ-GT were measured using commercially available kits (Nanjing Jiancheng Bioengineering Institute, Nanjing, China) following the manufacturer's instructions.

Determination of Inflammatory Cytokines. Expression levels of inflammatory factors, including interleukin-1β (IL-1β), interleukin-6 (IL-6), interleukin-10 (IL-10), and tumor necrosis factor-α (TNF-α), were detected by a commercially available enzyme-linked immunosorbent assay kit (Jingmei Biological Technology Co., Ltd., Jiangsu, China). The experiments were conducted exactly as outlined in the protocol provided by the kit manufacturer.

Determination of Oxidative Stress. Oxidative stress indicators, including glutathione (GSH), malondialdehyde (MDA), total superoxide dismutase (SOD), and catalase (CAT), were detected by different commercially available kits (Jiancheng Bioengineering Institute, Nanjing, China).

ROS and hepatocyte nucleus costaining immunofluorescence assay was used to detect the ROS level in the liver. Frozen sections of quail liver tissue were prepared beforehand, slightly dried, and added to the ROS dye solution. After the slices were slightly dried, the DAPI dye (Wuhan Servicebio Biotechnology Co., Ltd., China) was added and incubated at room temperature away from light. The DAPI dye was cleaned with PBS solution. The slices were dried slightly. The sections were then sealed with an antifade mounting medium (Servicebio Biotechnology Co., Ltd., Wuhan, China). The DAPI-stained nuclei appeared blue when exposed to ultraviolet light, while the positive expression was indicated by red fluorescence.

Histopathology and Ultrastructural Observation. The liver tissues were preserved using paraformaldehyde, dehydrated using a sequence of ethanol solutions with progressively higher concentrations and subsequently embedded in paraffin. Following this, the tissues were dewaxed using a sequence of ethanol solutions with progressively diminishing concentration levels and stained using hematoxylin and eosin (Servicebio Biotechnology Co., Ltd., Wuhan, China). The optical microscope was used to observe and take photographs of all sections (TE2000, Nikon, Japan). The researchers scored the liver sections in a blinded manner. The liver injury score was evaluated by the number percentage of cell necrosis, the area percentage of bleeding, inflammatory cell infiltration, and vacuolar degeneration. Each pathological index was scored on a scale of 0−3, without damage was scored as 0; damage degree <5% was scored as 1; damage degree 5−10% was scored as 2; damage degree >10% was scored as 3.[24] The tissue injury score was the sum of all scores.

https://doi.org/10.1021/acsomega.4c03767
ACS Omega 2024, 9, 25370−25380

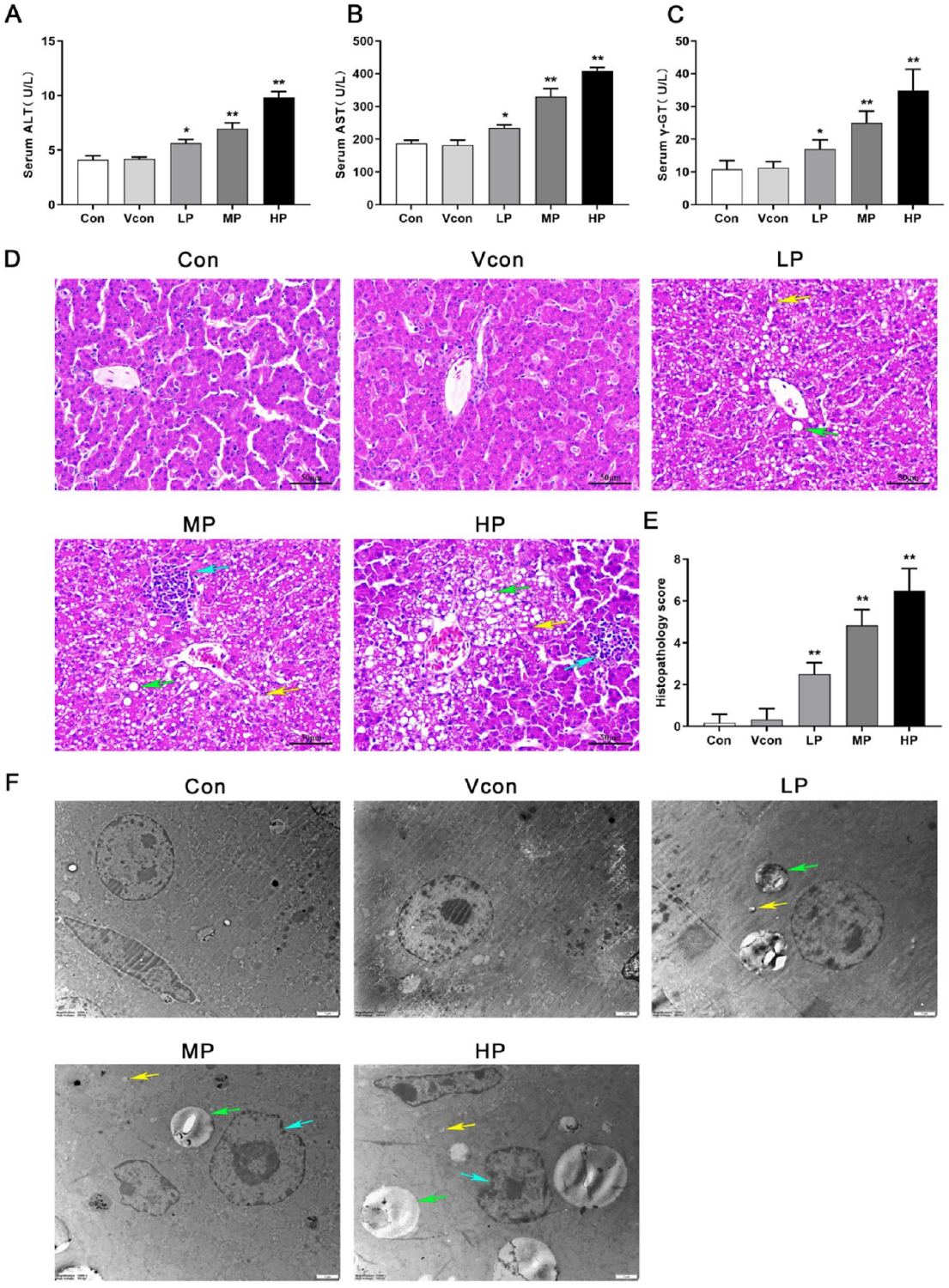

Figure 1. Effects of different concentrations of PFOS on liver function indexes and histopathology. The levels of serum (A) ALT, (B) AST, and (C) gamma-GT. B. (D) Liver H and E staining image, magnification: ×400. Scale bar = 50 μm. Green arrows indicate vacuolar degeneration; blue arrows indicate inflammatory cell infiltration, and yellow arrows indicate bleeding. (E) The liver injury score. (F) Ultrastructural examination of the liver. Yellow arrows indicate cavitation of mitochondria, blue arrows indicate the signature of apoptosis (nuclear membrane lysis), green arrows represent lipid, and scale bars = 1 μm. Data are expressed as mean ± SD (n = 6). *p < 0.05 and **p < 0.01 versus the Con group.

Following a 48-h fixation period using a 3% glutaraldehyde solution, small pieces of liver tissue (1 mm^3) were exposed to osmium tetroxide. The tissue blocks were then dehydrated, embedded, sliced, and stained with lead citrate. All the images were obtained through the utilization of a transmission electron microscope (H-7650, Hitachi, Japan).

Real-Time PCR Analysis. Liver tissue was subjected to total RNA extraction using a commercially available total RNA extraction kit (LS1040, Promega Biotechnology Co., Ltd., Beijing, China). Real-time PCR was used to analyze gene expression levels in liver tissues. The gene types and primers involved in this part are shown in Supporting Information

https://doi.org/10.1021/acsomega.4c03767
ACS Omega 2024, 9, 25370−25380

Table 1. To quantify relative mRNA expression, the cycle threshold (Ct) values of the target genes were normalized to the Ct values of reference gene GAPDH, and the results are presented as fold change using the $2^{-\Delta\Delta Ct}$ method. The PCR results were calculated using the following equations: $\Delta Ct = Ct_{target\ gene} - Ct_{GAPDH}$ and $\Delta\Delta Ct = \Delta Ct_{treated\ group} - \Delta Ct_{control\ group}$.

Western Blotting. The western blot technique was employed to ascertain the protein expression levels in liver tissue. The liquid portion of the liver tissue was obtained following the process of grinding and centrifugation. The concentration of proteins in the supernatant was measured using the BCA protein concentration determination kit (P0010S, Beyotime Biotechnology, Shanghai, China). The protein samples underwent separation through the use of SDS-PAGE gel electrophoresis, followed by their subsequent transfer onto PVDF membranes. 5% concentration of skim milk solution was prepared to block the PVDF membranes of the previous step for 2 h. Primary antibodies were diluted with primary antibody dilution buffer (Leagene Biotechnology, Beijing, China) at the appropriate dilution ratio. The required primary antibodies include anti-Bcl-2; anti-Bax; anti-cleaved caspase-3; anti-cleaved caspase-9; anti-TLR4; anti-TNF-α; anti-IL-1β; anti-IL-10; anti-histone H3; anti-GAPDH; anti-IL-6; anti-cytochrome C (the above antibodies were purchased from WanLei Biotechnology in Shenyang, China, and diluted 1:500); anti-NF-κB p65 (1:500, Bioss Biotechnology, Beijing, China); anti-P53 (1:1000, Bioss Biotechnology, Beijing, China); and anti-MyD88 (1:1000, Bioss Biotechnology, Beijing, China). The PVDF membranes were submerged in primary antibodies for an extended period at a temperature of 4 °C. The primary antibodies were eliminated through a rinsing process, the secondary antibodies were prepared and PVDF membranes were placed in it, and the dilution ratio of horseradish enzyme labeled goat antirabbit IgG was 1:20000 (ZSGB-BIO, Beijing, China). After a 2-h incubation period, the presence of all protein immunoblotting bands was detected using the ECL chemiluminescence substrate kit (Tanon Life Sciences Co., Ltd., Shanghai, China). Images were taken with a Tanon 5200 automatic chemiluminescence image analysis system and gray values of the bands were analyzed for quantification with ImageJ. The results of our study are presented in the form of a ratio of the intensity, which is calculated by dividing the intensity of the target protein bands by the intensity of the GAPDH band.

Immunohistochemistry Analysis. Paraffin sections were dewaxed twice in xylene, then dehydrated with absolute ethanol and gradient concentration ethanol solution, and finally rinsed with distilled water. The sections were evenly spread with 3% H_2O_2 and incubated, and then placed in citric acid antigen repair solution, microwave heated, and cooled naturally. The sections were then sealed with antibody homologous serum, and after that, the serum was removed after 30 min. Primary and secondary antibodies were added and incubated. They were removed and washed with PBS solution. DAB chromogenic reagent was added, followed by hematoxylin redyeing process and dehydration, and finally observed with a microscope (Olympus, Tokyo, Japan).

Apoptosis Detection. In quails, apoptosis was detected using a TUNEL Apoptosis Assay Kit (Roche, Basel, Switzerland) as per the manufacturer's instructions. Briefly, 50 μL of TdT and 450 μL of fluorescein-labeled dUTP reagents were mixed for all positive controls. Only 50 μL of the dUTP reagent was added to the negative control group. Each section received 50 μL of the TUNEL reaction mixture and was incubated at 37 °C for 1 h. After washing and drying, 50 μL of Converter-POD was added to liver tissue and incubated at 37 °C for 30 min. After rinsing, 50−100 μL of the DAB substrate was added and reacted for 10 min. Various sections were examined and imaged using a fluorescent inverted microscope (TE2000, Nikon, Japan). The apoptosis rate of 6 discontinuous regions/sections was calculated using ImageJ software.

Statistical Analysis. All data represent the mean ± standard error means (SEM) and were analyzed using Graph Pad Prism7 (Graphpad Software Inc., San Diego, USA). The statistical analysis for comparing multiple groups was conducted using a one-way analysis of variance (ANOVA) followed by a Tukey posthoc test. The mean integral optical density was determined using the Image-Pro Plus software (Media Cybernetics, Bethesda, MD, USA). $p < 0.05$ were considered statistically significant, and $p < 0.01$ were considered extremely significant.

RESULTS

Effects of Different Concentrations of PFOS on Liver Function, Histopathology, and Ultrastructure Observation. The three common liver function measures we measured are biomarkers of liver damage, with higher elevations indicating more severe damage. Compared with the Con group, the activity levels of AST, ALT, and γ-GT in the MP and HP groups were increased with the increase of PFOS concentration in the diet ($p < 0.05$, Figure 1A−C). H and E staining showed a radial arrangement of hepatic cords, no abnormal pathological changes were observed in the Con and Vcon groups, while obvious pathological changes were observed in the liver tissues of the MP and HP groups, such as disordered arrangement of hepatocytes, a certain amount of inflammatory cell infiltration, serious vacuolar degeneration and minor bleeding (Figure 1D). The liver injury scores of the quails in the LP, MP, and HP groups were higher than those of the CON group ($p < 0.01$; Figure 1E). These results were consistent with the liver function evaluation. Thus, the observation of H and E staining results showed that PFOS exposure to quail livers could lead to some serious pathological changes, which were related to the dose of PFOS exposure, and the higher the dose of PFOS, caused more serious damage.

The results of transmission electron microscopy analysis of liver ultrastructure showed that the nuclear membrane of hepatocytes in the Con group was intact, the distribution of nuclear cytoplasm was uniform, and the distribution of chromatin in the nucleus was normal, only a few cells were apoptotic (Figure 1F). The mitochondrial structure is complete, and the mitochondrial ridge structure inside is clear. In the MP and HP groups, irregular contraction and rupture of nuclei were observed, and internal chromatin was aggregated into clumps close to the nuclear membrane, showing typical apoptotic characteristics. The mitochondria outside the nucleus were vacuolated and swollen, and the inner bilayer structure and mitochondrial cristae were destroyed. Intracellular lipid accumulation was observed in all PFOS-exposed groups.

Determination of Oxidative Stress Indicators. The fluorescence detection results of ROS in liver tissue of quail in each group showed that the fluorescence intensity of the MP and HP groups was stronger than that of the Con and Vcon groups, and there was no significant increase in the LP group

https://doi.org/10.1021/acsomega.4c03767
ACS Omega 2024, 9, 25370−25380

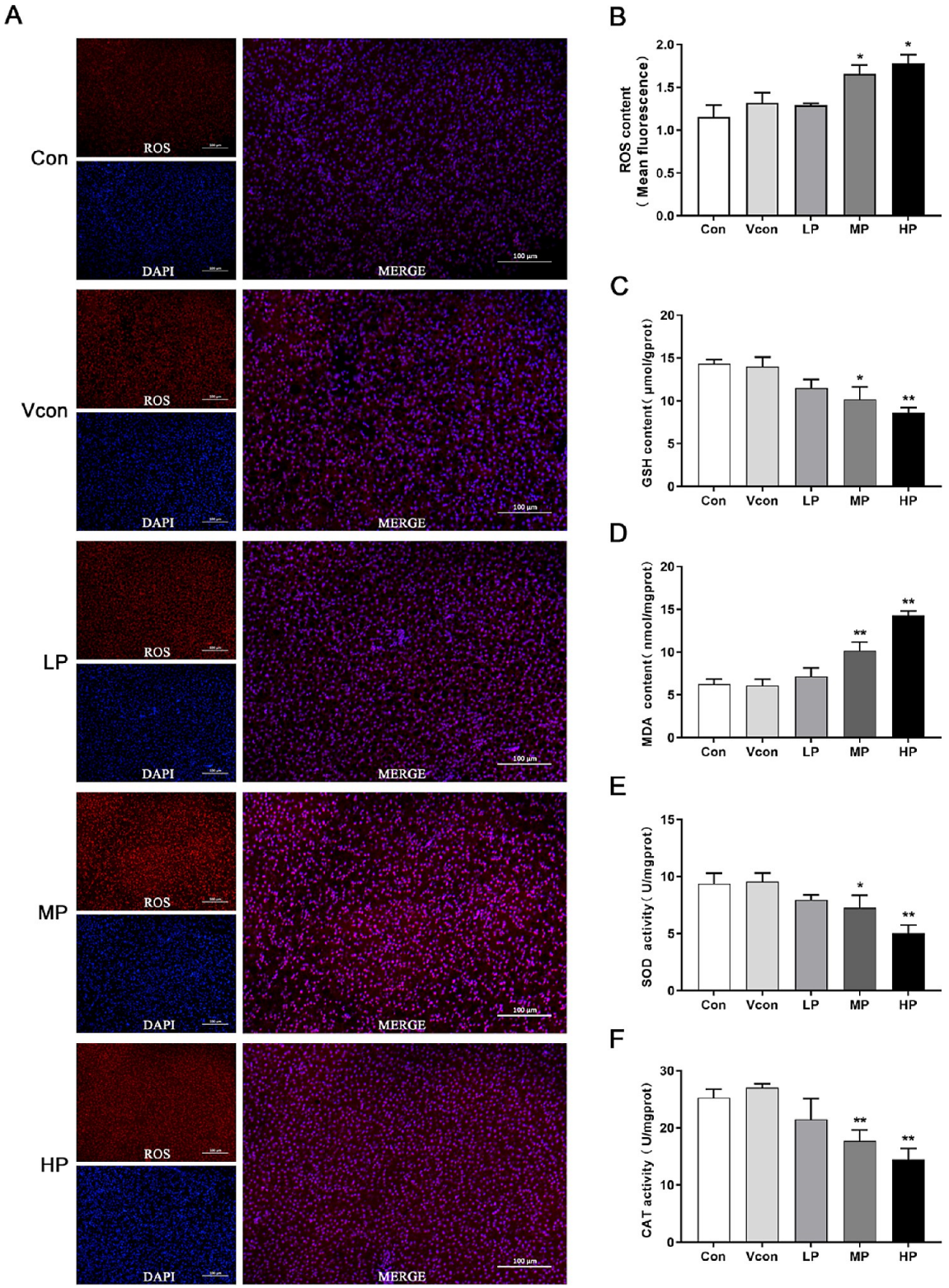

Figure 2. Determination of oxidative stress indices. (A) ROS immunofluorescence in hepatocytes and (B) mean fluorescence intensity of ROS in hepatocytes, magnification: ×200, scale bars = 100 μm. (C) GSH, (D) MDA, (E) SOD, and (F) CAT content in the liver. Data are expressed as mean ± SD (n = 6). *p < 0.05 and **p < 0.01 versus the Con group.

compared with the Con group, indicating that the higher the dose of PFOS exposure, the higher the fluorescence intensity of ROS (p < 0.05, Figure 2A). With the increase of PFOS dose, the content of GSH in the liver gradually decreased, and the activity of SOD and CAT decreased. On the contrary, the content of MDA increased (p < 0.05, Figure 2B–F). It can be seen that PFOS exposure can activate the production of pro-oxidation factors and reduce the content and activity of antioxidation factors, which can be observed in a dose-dependent manner.

https://doi.org/10.1021/acsomega.4c03767
ACS Omega 2024, 9, 25370−25380

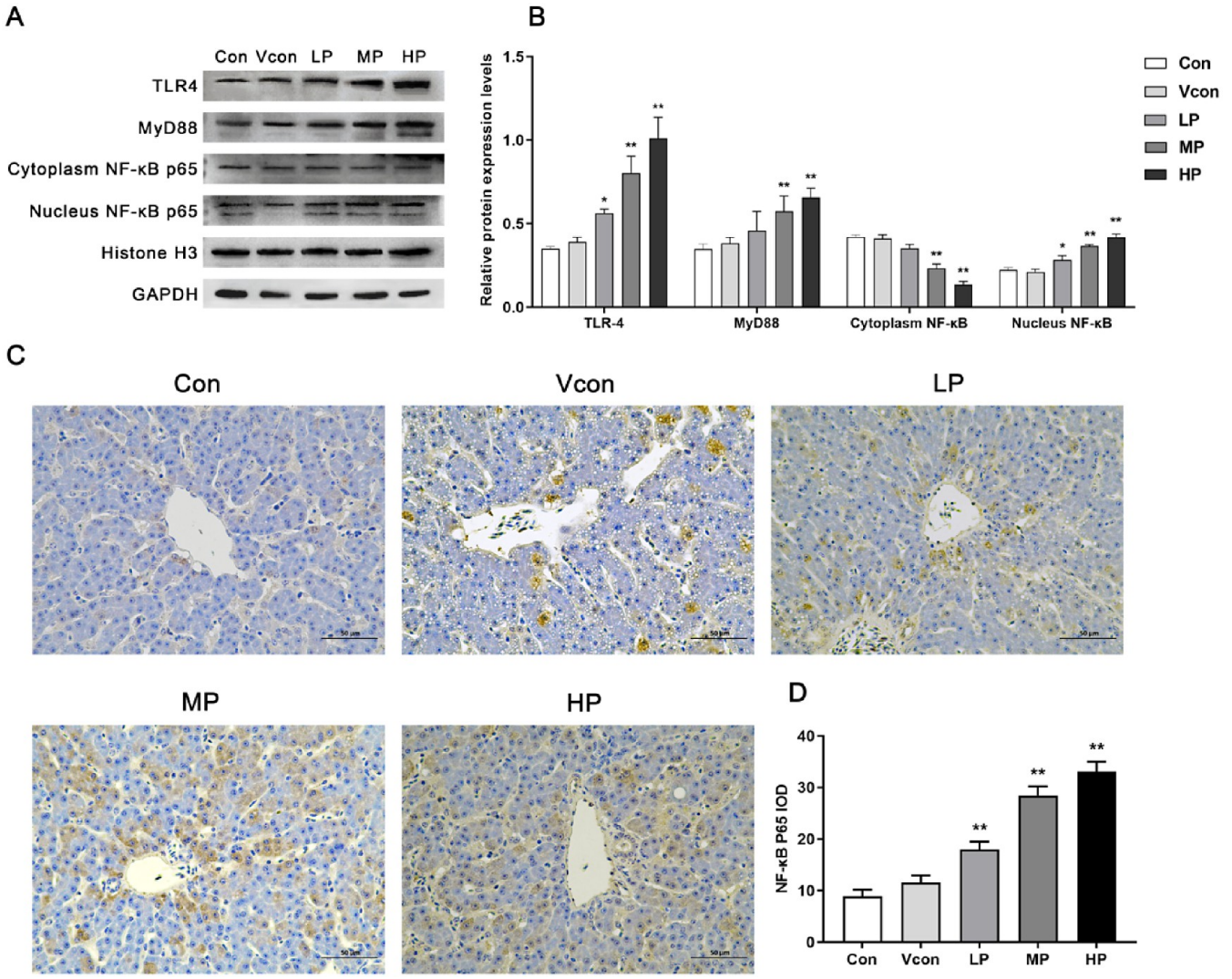

Figure 3. Effect of PFOS on the TLR4/Myd88/NF-κB signaling pathway. (A) Representative blots of TLR4, Myd88, cytoplasm NF-κB p65, and nucleus NF-κB p65. (B) Quantitative analysis of TLR4, Myd88, cytoplasm NF-κB p65, and nucleus NF-κB p65 proteins. Results are presented as the ratio of the intensity of the TLR4, Myd88, cytoplasm NF-κB p65, and nucleus NF-κB p65 bands to the intensity of the GAPDH band. (C) Immunohistochemistry images of NF-κB P65, magnification: ×400. Scale bars = 50 μm. (D) Quantitative analysis of immunohistochemistry of NF-κB P65. Data are expressed as mean ± SD (n = 6). *p < 0.05 and **p < 0.01 versus the Con group.

Effect of PFOS on the TLR4/Myd88/NF-κb Signaling Pathway. We found that PFOS dose-dependently increased the protein expression levels of TLR4, MyD88, and NF-κB p65 nucleoprotein, and on the contrary, the cytoplasmic protein expression level of NF-κB p65 decreased with the increase of PFOS dose (p < 0.05, Figure 3A,B). Immunohistochemical results showed that PFOS significantly increased the expression level of NF-κB p65 (Figure 3C,D). We found that PFOS can activate the TLR4/MyD88/NF-κB signaling pathway and trigger the nucleation of NF-κB to play its role.

Effects of Varying Concentrations of PFOS on the Levels of Hepatic Inflammatory Factors. We examined the levels of inflammatory factors in serum and found that PFOS significantly increased the IL-1β, IL-6, and TNF-α levels, and conversely decreased the IL-10 level (p < 0.05, Figure 4A−D). The effect of PFOS on the protein expression level of inflammatory factors in liver tissues increased with the increase of dose except IL-10 (p < 0.01, Figure 4E,F). We found that PFOS can enhance the presence of pro-inflammatory factors and inhibit anti-inflammatory factors, and the higher the concentration of PFOS, the more obvious this phenomenon is.

Effects of Different Concentrations of PFOS on Apoptosis of Hepatocytes. The outcomes of the TUNEL assay indicated that minimal green fluorescence was observed in the Con and Vcon groups, while green fluorescence was detected in all groups exposed to PFOS, with the intensity of fluorescence showing a direct relationship with the concentration of PFOS. Statistical analysis of the apoptosis rate of quail liver cells showed that compared with the Con group, the percentage of apoptotic cells in the LP group, MP group, and HP group increased with the increase of PFOS dose (p < 0.01, Figure 5A,B). PFOS dose-dependently increased the expression levels of Bax, cytochrome C, P53, caspase-3, and caspase-9 mRNA, and conversely decreased the expression level of Bcl-2 mRNA (p < 0.01, Figure 5C). PFOS dose-dependently increased the protein expression levels of Bax, cytochrome C, P53, cleaved caspase-3 and cleaved caspase-9 and decreased the protein expression level of Bcl-2. Moreover, the ratio of Bax to Bcl-2 protein expression level increased with

https://doi.org/10.1021/acsomega.4c03767
ACS Omega 2024, 9, 25370−25380

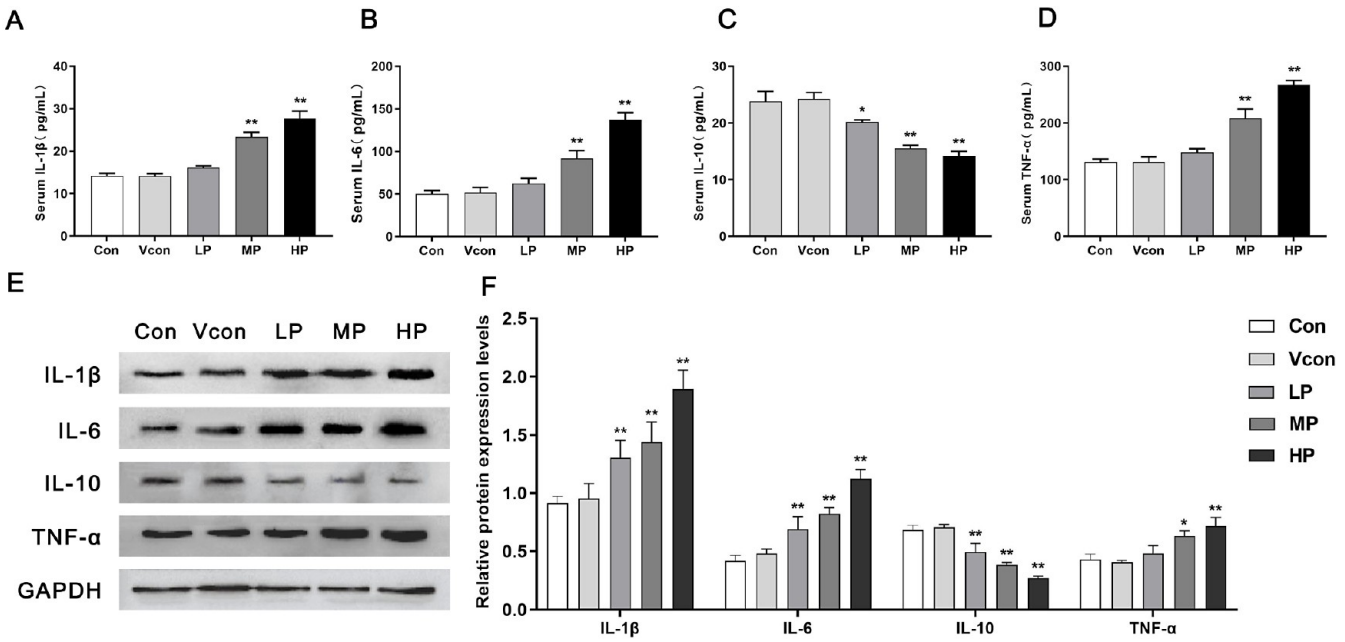

Figure 4. Effects of different concentrations of PFOS on the levels of hepatic inflammatory factors. (A) Serum IL-1β, (B) IL-6, (C) IL-10, and (D) TNF-α content. (E) Representative blots of IL-1β, IL-6, IL-10, and TNF-α. (F) Quantitative analysis of IL-1β, IL-6, IL-10, and TNF-α proteins. Results are presented as the ratio of the intensity of the IL-1β, IL-6, IL-10, and TNF-α bands to the intensity of the GAPDH band. Data are expressed as mean ± SD (n = 6). *p < 0.05 and **p < 0.01 versus the Con group.

the increase of PFOS dose (p < 0.05, Figure 5D). Immunohistochemical results showed that PFOS increased the expression levels of P53 and cleaved caspase-3 (p < 0.01, Figure 6A–D). We found that PFOS induced apoptosis of quail liver cells through the mitochondrial pathway, and the severity of apoptosis was positively correlated with the dose of PFOS exposed.

DISCUSSION

PFOS can cause toxic reactions in various body systems and organs. Due to its stable chemical properties and difficulty metabolizing, PFOS' toxic effects are stable and long-lasting. The damage PFOS causes is closely related to the total amount entering a single organism.[25] Before this study, a reasonable PFOS concentration gradient must be designed to ensure experiment continuity with most experimental animals surviving. It was found that the median lethal dose (LD_{50}) of PFOS for a variety of avian species, among which the LD_{50} of juvenile quail was 61 mg/kg of PFOS given per day.[26] Three groups of different PFOS concentrations were determined by calculation based on average quail body weight and daily feed consumption. No experimental quail died during PFOS administration.

The liver is the primary site of PFOS accumulation in humans and animals and is also the primary organ of metabolism and detoxification. Our results preliminarily confirmed the hepatotoxicity of PFOS, evidenced by elevated serum ALT and AST levels in PFOS-exposed quail and a positive correlation with PFOS concentration. Once the liver is damaged, ALT and AST enter the bloodstream; these two indicators are suggestive of liver disease.[27] Upon examination of hepatocyte subcellular structure via transmission electron microscopy, we observed varying degrees of damage to both the cytomembrane and mitochondria. ALT and AST are distributed differently in hepatocytes. ALT is primarily distributed in the liver cytoplasm; its elevation reflects hepatocyte membrane damage. AST is predominantly distributed in hepatocyte plasma and mitochondria; its elevation suggests hepatocyte organelle injury. γ-GT in serum is mainly from the liver and gallbladder. The increase of γ-GT in serum indicates liver damage.[28] Additionally, PFOS induced overt tissue vacuolation, cell necrosis, hepatic sinus hemorrhage, and inflammatory cell infiltration in HE-stained liver sections, evidencing liver damage.

PFOS is considered a hepatotoxin, potentially causing liver injury via oxidative stress. This stress arises from the overproduction of reactive oxygen species (ROS). Mitochondria are prime targets of exogenous toxins; their dysfunction induces various liver diseases and ROS overproduction.[29] The imbalance between ROS production and antioxidants triggers oxidative stress.[30] ROS acts as a vital second messenger in numerous intracellular signaling cascades, helping maintain homeostasis.[31] SOD GSH are major antioxidants. With CAT, they mitigate oxidative damage by scavenging ROS.[32] Malondialdehyde (MDA) content indicates potential antioxidant capacity and lipid peroxidation rate, indirectly reflecting tissue damage extent.[33] This study found PFOS damaged mitochondrial structure, suggesting potential functional impairment. Therefore, we detected ROS levels and oxidative stress markers in hepatocytes. Moderate and high PFOS doses significantly increased ROS and MDA while downregulating antioxidants like GSH. These results indicate that PFOS induces free radical production and weakens antioxidant defenses to induce hepatotoxicity in quails.

NF-κB is the most critical point in the signaling pathway related to the inflammatory response pathway in hepatocytes.[34] NF-κB is typically found within the cytoplasmic compartment. Released after degradation, NF-κB enters the nucleus and regulates the expression level of anti-inflammatory/pro-inflammatory factors (anti-inflammatory such as IL-10, pro-inflammatory such as IL-1β and IL-6) to regulate the inflammatory response of cells.[35] Many factors can trigger

https://doi.org/10.1021/acsomega.4c03767
ACS Omega 2024, 9, 25370−25380

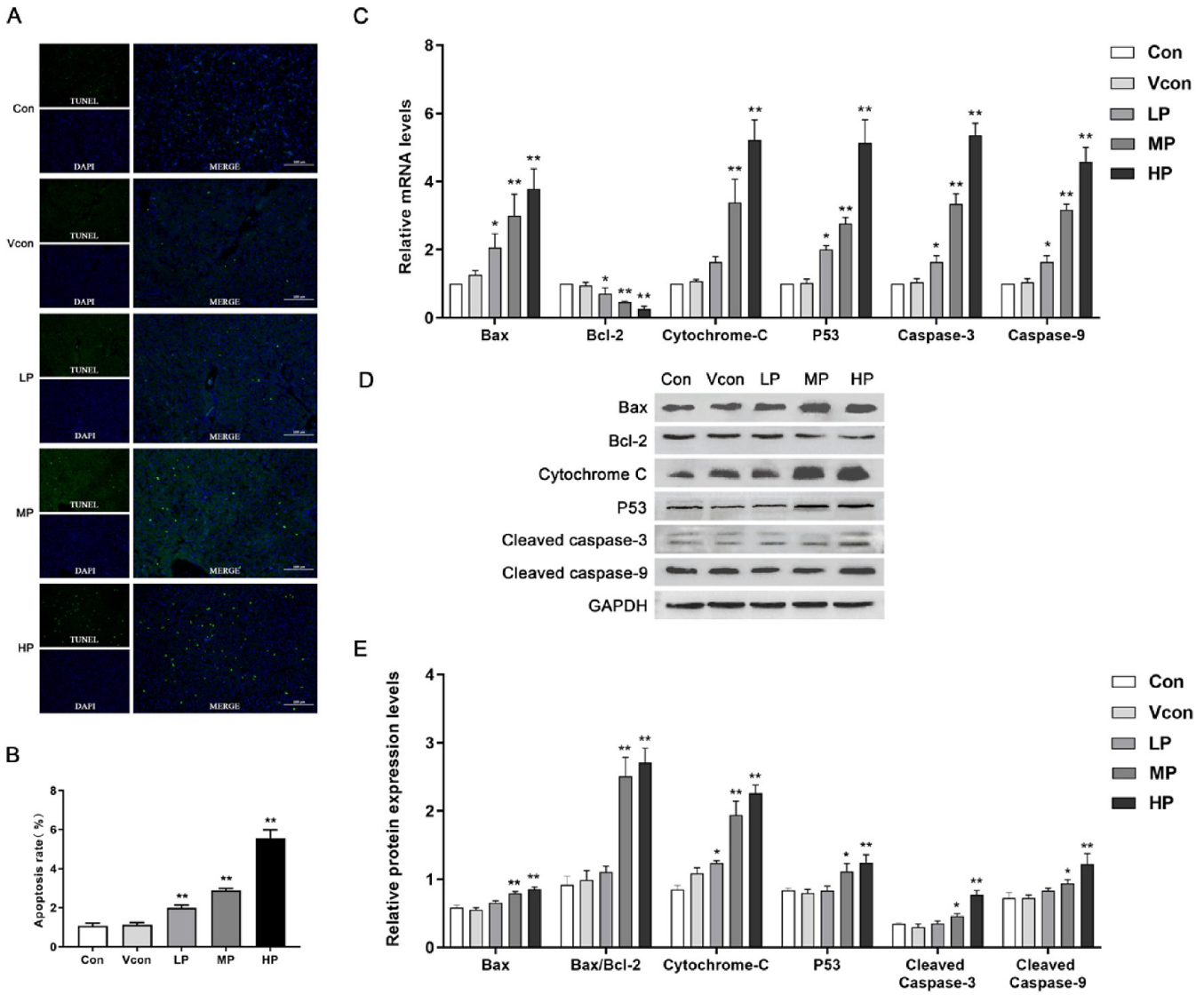

Figure 5. Effects of different concentrations of PFOS on apoptosis of hepatocytes. (A) Representative TUNEL images and the apoptosis rate, magnification: ×200, scale bars = 100 μm. (B) The apoptosis rate was assessed. (C) The expression levels of Bax, Bcl-2, cytochrome C, P53, caspase-3, and caspase-9 mRNA. (D) Representative blots of Bax, Bcl-2, cytochrome C, P53, cleaved caspase-3, and cleaved caspase-9 and immunohistochemistry images of P53. (E) Quantitative analysis of Bax, Bcl-2, cytochrome C, P53, cleaved caspase-3, and ceaved caspase-9 proteins. Results are presented as the ratio of the intensity of the Bax, Bcl-2, cytochrome C, P53, cleaved caspase-3, and cleaved caspase-9 bands to the intensity of the GAPDH band. Data are expressed as mean ± SD (n = 6). *p < 0.05 and **p < 0.01 versus the Con group.

the activation of NF-κB signaling pathway, such as some inflammatory factors (IL-1, TNF-α), growth factors (TGF-α, etc.), and lipopolysaccharide (LPS). The TLR4/NF-κB signaling pathway is a well-established and widely recognized inflammatory signaling pathway in the field of immunology. TLR4 can activate the over release of various inflammatory factors and immunomodulatory cytokines such as IL-1β, TNF-α, IL-6, and IL-10 through its downstream MyD88-dependent and non-MyD88-dependent signaling pathways.[36] Mice with MyD88 gene knockout can still induce MyD88-dependent and independent TLR4 signal transduction pathway activity, and the activation of NF-κB is delayed compared with those without knockout, indicating that MyD88 is an important link in the early response process of TLR4 signal transduction pathway.[37] Some studies have found that PFOS could cause inflammation. We found that PFOS administration caused significant histopathological changes in the liver of quail, especially the infiltration of inflammatory cells. PFOS treatment resulted in significant NF-κB activation, and increased expression of NF-κB P65 nucleoprotein in the liver demonstrated the role of NF-κB P65 through its entry into the nucleus. In addition, the increased expression levels of TLR4 and MyD88 indicated that PFOS activated the TLR4/MyD88/NF-κB signaling pathway. The protein expression levels and serum contents of inflammatory factors IL-1β, IL-6, and TNF-α increased, and the anti-inflammatory factor IL-10 decreased, indicating that PFOS aggravated liver inflammation and inhibited the anti-inflammatory ability of hepatocytes with the increase in concentration. In addition, the TLR4/MyD88/NF-κB signaling pathway can be activated by excessive ROS generation, which can worsen the inflammatory response.[38] Excessive ROS can lead to cellular damage and induction of the NF-κB inflammatory pathway in liver injury.[39] Thus, PFOS induces hepatotoxicity in quails by exacerbating oxidative stress and inflammation through activating TLR4/MyD88/NF-κB signaling.

https://doi.org/10.1021/acsomega.4c03767
ACS Omega 2024, 9, 25370−25380

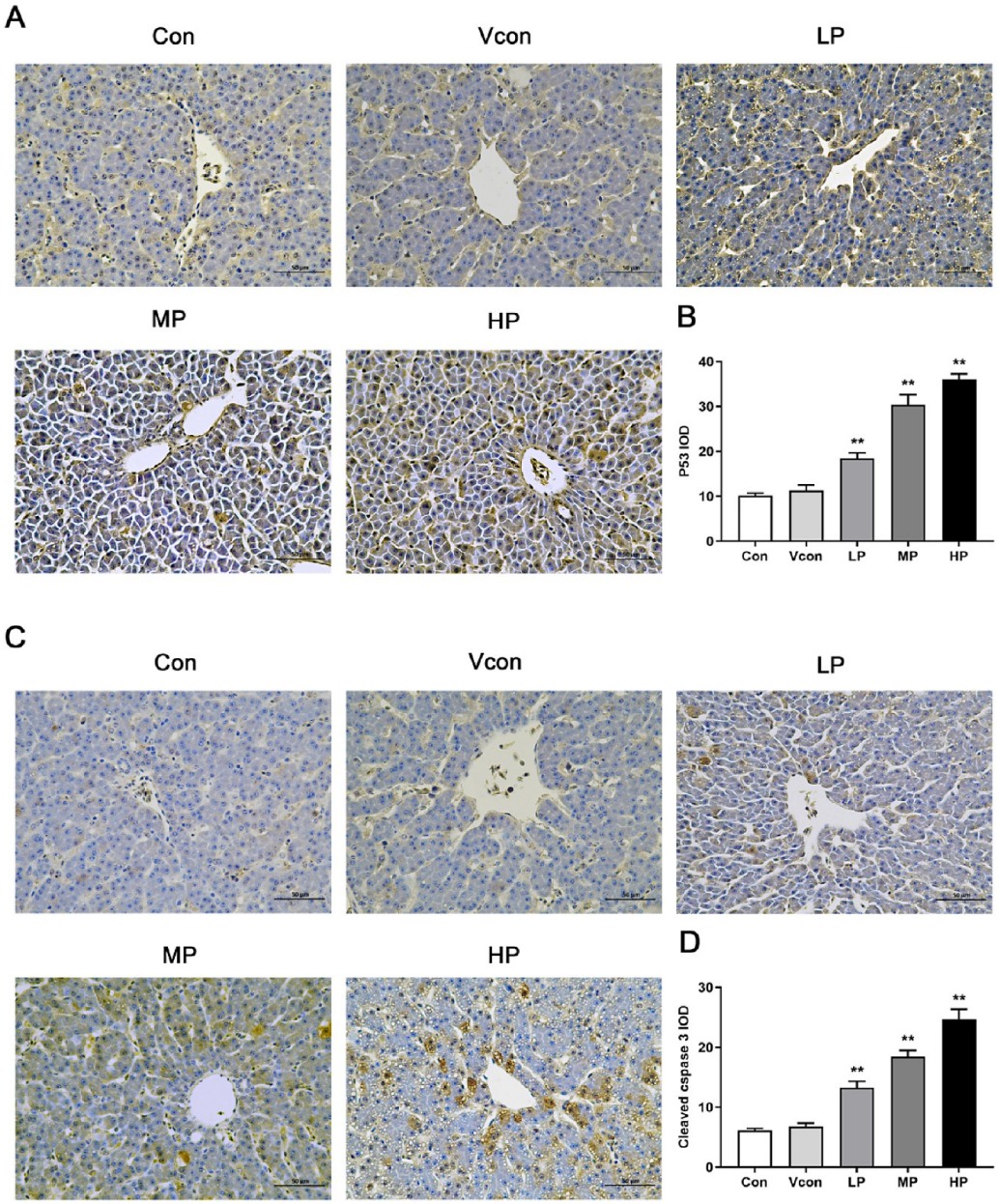

Figure 6. Immunohistochemistry images of (A) P53 and (C) cleaved caspase-3. magnification: × 400. Quantitative analysis of immunohistochemistry of (B) P53 and (D) cleaved caspase-3. Scale bars = 50 μm. Data are expressed as mean ± SD (n = 6). *p < 0.05 and **p < 0.01 versus the CON group.

Apoptosis is a regulated, genetically controlled process of cell death in multicellular organisms. Both inflammation and oxidative stress can trigger apoptosis of liver cells.[40] We found that moderate and high doses of PFOS significantly induced quail hepatocyte apoptosis, preliminarily indicated by increased cells undergoing apoptosis within a given area. In our study, the mitochondrial pathway is considered a common path of apoptosis. Upon mitochondrial damage and dysfunction, Bax translocates from the cytoplasmic compartment to the outer mitochondrial membrane, where it intercalates and forms oligomers. Bax oligomerization triggers the release of cytochrome c and other apoptotic factors. Released into the cytoplasm, cytochrome c binds to Apaf-1 to activate caspase-9. Bcl-2 has been shown to prevent apoptosis induced by various stimuli. Bcl-2 and Bcl-xL, belonging to the same family, are situated within the mitochondrial, endoplasmic reticulum, and nuclear membranes, preventing the release of apoptotic factors from mitochondria, e.g., preventing cytochrome C entry into the cytoplasm from the mitochondrial intermembrane space.[41] Bcl-2 suppresses the function of Bax through the formation of a heterodimeric complex with the pro-apoptotic protein Bax. When Bax/Bcl-2 is upregulated by certain factors, caspase-3 is activated in the form of cleavage.[42] P53 plays a crucial role in regulating apoptosis triggered by DNA damage. In the context of DNA damage, p53 undergoes prompt phosphorylation by kinases associated with phosphoinositide 3-kinase. Subsequently, Bax/Bcl-2 is upregulated due to p53 activation.[43] As cytochrome C is a marker of mitochondrial apoptosis and mitochondrial structure disruption has been observed, we examined cytochrome C levels in liver tissue to determine if mitochondrial apoptosis occurred. We found different PFOS concentrations upregulated expression of P53, cytochrome C,

https://doi.org/10.1021/acsomega.4c03767
ACS Omega 2024, 9, 25370−25380

caspase-3, and caspase-9 and the Bax/Bcl-2 ratio. Furthermore, apoptosis was driven by rising ROS levels from PFOS. Thus, PFOS induced apoptosis in quail hepatocytes through the mitochondrial pathway, with severity closely related to dose.

In summary, PFOS induces mitochondrial apoptosis by exacerbating oxidative stress and inflammation by activating the TLR4/MyD88/NF-κB signaling pathway, ultimately leading to hepatotoxicity in quails. The findings show liver damage from PFOS exposure and related mechanisms, providing evidence and new perspectives for research on harm from industrial pollutants in humans and animals.

■ ASSOCIATED CONTENT

Data Availability Statement

All data generated for the current study are included in the manuscript and Supporting Information.

Supporting Information

The Supporting Information is available free of charge at https://pubs.acs.org/doi/10.1021/acsomega.4c03767.

The appearance and dimensions of quail livers (Supporting Information Figure 1) and primer sequences for real-time PCR detection (Supporting Information Table 1) (PDF)

■ AUTHOR INFORMATION

Corresponding Authors

Tianyuan Yang − *College of Veterinary Medicine, Northeast Agricultural University, Harbin, Heilongjiang 150030, China*; Email: qqqwww0409@163.com

Shuai Zhang − *College of Veterinary Medicine, Northeast Agricultural University, Harbin, Heilongjiang 150030, China*; orcid.org/0000-0002-7876-5578; Email: zhangshuai19900322@gmail.com

Authors

Jiucheng Wang − *College of Veterinary Medicine, Northeast Agricultural University, Harbin, Heilongjiang 150030, China*

Zanyu Wang − *College of Veterinary Medicine, Northeast Agricultural University, Harbin, Heilongjiang 150030, China; Heilongjiang Provincial Agricultural Products and Veterinary Medicine Feed Technology Appraisal Station, Harbin, Heilongjiang 150008, China*

Yulin Tang − *College of Veterinary Medicine, Northeast Agricultural University, Harbin, Heilongjiang 150030, China*

Yuan Zhao − *College of Veterinary Medicine, Northeast Agricultural University, Harbin, Heilongjiang 150030, China*

Hao Fang − *College of Optoelectronic Engineering, Chongqing University, Chongqing, Sichuan 400044, China*

Yuntong Zhang − *College of Veterinary Medicine, Northeast Agricultural University, Harbin, Heilongjiang 150030, China*

Xiaoyu Hou − *College of Veterinary Medicine, Northeast Agricultural University, Harbin, Heilongjiang 150030, China*

Haoyang Tan − *College of Veterinary Medicine, Northeast Agricultural University, Harbin, Heilongjiang 150030, China*

Shiming Yu − *College of Veterinary Medicine, Northeast Agricultural University, Harbin, Heilongjiang 150030, China*

Haiyang Zhang − *College of Veterinary Medicine, South China Agricultural University, Guangzhou, Guangdong 510642, China*; orcid.org/0000-0002-5935-8053

Honggang Fan − *College of Veterinary Medicine, Northeast Agricultural University, Harbin, Heilongjiang 150030, China*; orcid.org/0000-0002-7671-6908

Complete contact information is available at: https://pubs.acs.org/10.1021/acsomega.4c03767

Author Contributions

#J.W. and Z.W. contributed equally to this work. All authors have read and agreed to the published version of the manuscript. S.Z., Honggang Fan, and T.Y. contributed to conceptualization; J.W., S.Z., and Z.W. contributed to writing; J.W., Z.W., and Hao Fang contributed to data analysis; Y.T., Yuan Zhao, Yuntong Zhang, X.H., H.T., S.Y., and H.Z. performed experiments; S.Z., Hao Fang, and T.Y. contributed to review and editing; all authors have read and agreed to the published version of the manuscript.

Notes

The authors declare no competing financial interest.

■ ACKNOWLEDGMENTS

This work was supported by the National Natural Science Foundation of China (grant no. 32373085 and grant no. 32273078) and the National Key R&D Program of China (grant no. 2023YFD1801104).

■ REFERENCES

(1) Panieri, E.; Baralic, K.; Djukic-Cosic, D.; Buha Djordjevic, A.; Saso, L. PFAS Molecules: A Major Concern for the Human Health and the Environment. *Toxics* **2022**, *10* (2), 44.

(2) Chen, H.; Gao, Y.; Mruk, D. D.; Xiao, X.; John, C. M.; Turek, P. J.; Lui, W.-Y.; Lee, W. M.; Silvestrini, B.; Cheng, C. Y. Rescue of PFOS-induced human Sertoli cell injury by overexpressing a p-FAK-Y407E phosphomimetic mutant. *Sci. Rep.* **2017**, *7* (1), 15810.

(3) Huang, S.; Jaffé, P. AcidimicrobiumDefluorination of Perfluorooctanoic Acid (PFOA) and Perfluorooctane Sulfonate (PFOS) by sp. *Strain A6. Environ. Sci. Technol.* **2019**, *53* (19), 11410−11419.

(4) Wei, C.; et al. Sorption kinetics, isotherms and mechanisms of PFOS on soils with different physicochemical properties. *Ecotoxicol. Environ. Saf.* **2017**, *142*, 40−50.

(5) Zhang, Z.; Wang, F.; Zhang, Y.; Yao, J.; Bi, J.; He, J.; Zhang, S.; Wei, Y.; Guo, H.; Zhang, X.; He, M. Associations of serum PFOA and PFOS levels with incident hypertension risk and change of blood pressure levels. *Environ. Res.* **2022**, *212* (Pt B), 113293.

(6) Lau, C.; et al. Perfluoroalkyl acids: a review of monitoring and toxicological findings. *Toxicol. Sci.* **2007**, *99* (2), 366−394.

(7) Chen, J.; et al. Chronic PFOS Exposure Disrupts Thyroid Structure and Function in Zebrafish. *Bull. Environ. Contam. Toxicol.* **2018**, *101* (1), 75−79.

(8) Cheng, W.; et al. Perfluorooctane sulfonate (PFOS) induced embryotoxicity and disruption of cardiogenesis. *Toxicol. In Vitro* **2013**, *27* (5), 1503−1512.

(9) Giesy, J. P.; Kannan, K. Global distribution of perfluorooctane sulfonate in wildlife. *Environ. Sci. Technol.* **2001**, *35* (7), 1339−1342.

(10) Kannan, K.; et al. Concentrations of perfluorinated acids in livers of birds from Japan and Korea. *Chemosphere* **2002**, *49* (3), 225−231.

(11) Kannan, K.; et al. Perfluorooctane sulfonate in fish-eating water birds including bald eagles and albatrosses. *Environ. Sci. Technol.* **2001**, *35* (15), 3065−3070.

(12) Perez, F.; et al. Accumulation of perfluoroalkyl substances in human tissues. *Environ. Int.* **2013**, *59*, 354−362.

(13) Kim, H.; et al. Induction of apoptosis and CYP4A1 expression in Sprague-Dawley rats exposed to low doses of perfluorooctane sulfonate. *J. Toxicol. Sci.* **2011**, *36* (2), 201−210.

(14) Franco, M.; Sutherland, G. E.; Fernandez-Luna, M. T.; Lavado, R. Altered expression and activity of phase I and II biotransformation enzymes in human liver cells by perfluorooctanoate (PFOA) and perfluorooctane sulfonate (PFOS). *Toxicology* **2020**, *430*, 152339.

(15) Li, X.; Li, T.; Wang, Z.; Wei, J.; Liu, J.; Zhang, Y.; Zhao, Z. Distribution of perfluorooctane sulfonate in mice and its effect on liver lipidomic. *Talanta* **2021**, *226*, 122150.
(16) Guo, J.; et al. The PFOS disturbed immunomodulatory functions via nuclear Factor-kappaB signaling in liver of zebrafish (Danio rerio). *Fish Shellfish Immunol.* **2019**, *91*, 87−98.
(17) Wang, L.; Wang, Y.; Liang, Y.; Li, J.; Liu, Y.; Zhang, J.; Zhang, A.; Fu, J.; Jiang, G. PFOS induced lipid metabolism disturbances in BALB/c mice through inhibition of low density lipoproteins excretion. *Sci. Rep.* **2014**, *4* (1), 4582.
(18) Huang, T.; Zhang, Y.; Zhang, W.; Lin, T.; Chen, L.; Yang, B.; Wu, L.; Yang, J.; Z.hang, D. Attenuation of Perfluorooctane Sulfonate-Induced Steatohepatitis by Grape Seed Proanthocyanidin Extract in Mice. *BioMed. Res. Int.* **2020**, *2020*, 8818160.
(19) Li, X.; Zhang, Q.; Wang, A.; Shan, S.; Wang, X.; Wang, Y.; Wan, J.; Ning, P.; Hong, C.; Tian, H.; Zhao, Y. Hepatotoxicity induced in rats by chronic exposure to F−53B, an emerging replacement of perfluorooctane sulfonate (PFOS). *Environ. Pollut.* **2024**, *346*, 123544.
(20) Chen, X.; Nie, X.; Mao, J.; Zhang, Y.; Yin, K.; Sun, P.; Luo, J.; Liu, Y.; Jiang, S.; Sun, L. Perfluorooctane sulfonate mediates secretion of IL-1β through PI3K/AKT NF-κB pathway in astrocytes. *Neurotoxicol. Teratol.* **2018**, *67*, 65−75.
(21) Zeng, H. C.; Zhu, B.-Q.; Wang, Y.-Q.; He, Q.-Z. ROS-Triggered Autophagy Is Involved in PFOS-Induced Apoptosis of Human Embryo Liver L-02 Cells. *BioMed. Res. Int.* **2021**, *2021*, 6625952.
(22) Sun, P.; Gu, L.; Luo, J.; Qin, Y.; Sun, L.; Jiang, S. ROS-mediated JNK pathway critically contributes to PFOS-triggered apoptosis in SH-SY5Y cells. *Neurotoxicol. Teratol.* **2019**, *75*, 106821.
(23) Sinha, K.; et al. Oxidative stress: the mitochondria-dependent and mitochondria-independent pathways of apoptosis. *Arch. Toxicol.* **2013**, *87* (7), 1157−1180.
(24) Li, L.; et al. Paeoniflorin ameliorates lipopolysaccharide-induced acute liver injury by inhibiting oxidative stress and inflammation via SIRT1/FOXO1a/SOD2 signaling in rats. *Phytother. Res.* **2022**, *36* (6), 2558−2571.
(25) Xing, J.; et al. Toxicity assessment of perfluorooctane sulfonate using acute and subchronic male C57BL/6J. mouse models. *Environ. Pollut.* **2016**, *210*, 388−396.
(26) Newsted, J.; et al. Avian toxicity reference values for perfluorooctane sulfonate. *Environ. Sci. Technol.* **2005**, *39* (23), 9357−9362.
(27) Ekser, B.; Gridelli, B.; Cooper, D. K. C. Porcine alanine transaminase after liver allo-and xenotransplantation. *Xenotransplantation* **2012**, *19* (1), 52−55.
(28) Bozkus, F.; et al. Serum Gamma-Glutamyl Transferase Activity as a Potential Novel Cardiovascular Biomarker in COPD. *Respir. Care* **2016**, *61* (11), 1465−1471.
(29) Sena, L.; Chandel, N. Physiological roles of mitochondrial reactive oxygen species. *Mol. Cell* **2012**, *48* (2), 158−167.
(30) Li, P.; Chang, M. Roles of PRR-Mediated Signaling Pathways in the Regulation of Oxidative Stress and Inflammatory Diseases. *Int. J. Mol. Sci.* **2021**, *22* (14), 7688.
(31) Cadenas, E.; Davies, K. Mitochondrial free radical generation, oxidative stress, and aging. *Free Radical Biol. Med.* **2000**, *29*, 222−230.
(32) Powers, S.; Lennon, S. Analysis of cellular responses to free radicals: focus on exercise and skeletal muscle. *Proc. Nutr. Soc.* **1999**, *58* (4), 1025−1033.
(33) Li, X.; et al. Bacillus amyloliquefaciens B10 can alleviate liver apoptosis and oxidative stress induced by aflatoxin B1. *Food Chem. Toxicologyan* **2021**, *151*, 112124.
(34) Yang, Y.; Kim, S.; Seki, E. Inflammation and Liver Cancer: Molecular Mechanisms and Therapeutic Targets. *Semin. Liver Dis.* **2019**, *39* (1), 26−42.
(35) Birbach, A.; et al. Signaling molecules of the NF-kappa B pathway shuttle constitutively between cytoplasm and nucleus. *J. Biol. Chem.* **2002**, *277* (13), 10842−10851.
(36) Yang, Y.; et al. Cloning and functional characterization of IRAK1 from rainbow trout (Oncorhynchus mykiss). *Dev. Comp. Immunol.* **2021**, *114*, 103780.
(37) Jiang, Z.; et al. Poly(I-C)-induced Toll-like receptor 3 (TLR3)-mediated activation of NFkappa B and MAP kinase is through an interleukin-1 receptor-associated kinase (IRAK)-independent pathway employing the signaling components TLR3-TRAF6-TAK1-TAB2-PKR. *J. Biol. Chem.* **2003**, *278* (19), 16713−16719.
(38) Liu, X.; et al. Amorphous silica nanoparticles induce inflammation via activation of NLRP3 inflammasome and HMGB1/TLR4/MYD88/NF-kb signaling pathway in HUVEC cells. *J. Hazard. Mater.* **2021**, *404*, 124050.
(39) Nowak, A. J.; Relja, B. The Impact of Acute or Chronic Alcohol Intake on the NF-κB Signaling Pathway in Alcohol-Related Liver Disease. *Int. J. Mol. Sci.* **2020**, *21* (24), 9407.
(40) Choudhury, S.; et al. Pomegranate protects against arsenic-induced p53-dependent ROS-mediated inflammation and apoptosis in liver cells. *J. Nutr. Biochem.* **2016**, *38*, 25−40.
(41) Wei, Q.; et al. Bax and Bak have critical roles in ischemic acute kidney injury in global and proximal tubule-specific knockout mouse models. *Kidney Int.* **2013**, *84* (1), 138−148.
(42) Zhu, L.; et al. Curcumin triggers apoptosis via upregulation of Bax/Bcl-2 ratio and caspase activation in SW872 human adipocytes. *Mol. Med. Rep.* **2015**, *12* (1), 1151−1156.
(43) Jiang, Y.; et al. BaP-induced DNA damage initiated p53-independent necroptosis via the mitochondrial pathway involving Bax and Bcl-2. *Hum. Exp. Toxicol.* **2013**, *32* (12), 1245−1257.

https://doi.org/10.1021/acsomega.4c03767
ACS Omega 2024, 9, 25370−25380